Theoretical and Experimental Studies of the Spin Trapping of Inorganic Radicals by 5,5-Dimethyl-1-Pyrroline *N*-Oxide (DMPO). 2. Carbonate Radical Anion

Frederick A. Villamena,*,† Edward J. Locigno,† Antal Rockenbauer,‡ Christopher M. Hadad,*,§ and Jay L. Zweier*,†

Center for Biomedical EPR Spectroscopy and Imaging, The Davis Heart and Lung Research Institute, the Division of Cardiovascular Medicine, Department of Internal Medicine, College of Medicine, the Department of Chemistry, The Ohio State University, Columbus, Ohio, 43210 and Chemical Research Center, Institute for Structural Chemistry, H-1025 Budapest, Pusztaszeri ut 59, Hungary

Received: September 1, 2006; In Final Form: October 13, 2006

Previous studies have shown that the enzyme-mediated generation of carbonate radical anion ($CO_3^{\bullet-}$) may play an important role in the initiation of oxidative damage in cells. This study explored the thermodynamics of $CO_3^{\bullet-}$ addition to 5,5-dimethyl-1-pyrroline *N*-oxide (DMPO) using density functional theory at the B3LYP/6-31+G**//B3LYP/6-31G* and B3LYP/6-311+G* levels with the polarizable continuum model to simulate the effect of the bulk dielectric effect of water on the calculated energetics. Theoretical data reveal that the addition of $CO_3^{\bullet-}$ to DMPO yields an O-centered radical adduct (DMPO−OCO_2) as governed by the spin (density) population on the $CO_3^{\bullet-}$. Electron paramagnetic resonance spin trapping with the commonly used spin trap, DMPO, has been employed in the detection of $CO_3^{\bullet-}$. UV photolysis of H_2O_2 and DMPO in the presence of sodium carbonate (Na_2CO_3) or sodium bicarbonate ($NaHCO_3$) gave two species (i.e., DMPO−OCO_2 and DMPO−OH) in which the former has hyperfine splitting constant values of $a_N = 14.32$ G, $a_{\beta-H} = 10.68$ G, and $a_{\gamma-H} = 1.37$ G and with a shorter half-life compared to DMPO−OH. The origin of the DMPO−OH formed was experimentally confirmed using isotopically enriched $H_2{}^{17}O_2$ that indicates direct addition of $HO^{\bullet}$ to DMPO. Theoretical studies on other possible pathways for the formation of DMPO−OH from DMPO−OCO_2 in aqueous solution and in the absence of free $HO^{\bullet}$ such as in the case of enzymatically generated $CO_3^{\bullet-}$, show that the preferred pathway is via nucleophilc substitution of the carbonate moiety by H_2O or HO^-. Nitrite formation has been observed as the end product of $CO_3^{\bullet-}$ trapping by DMPO and is partly dependent on the basicity of solution. The thermodynamic behavior of $CO_3^{\bullet-}$ in the aqueous phase is predicted to be similar to that of the hydroperoxyl ($HO_2^{\bullet}$) radical.

Introduction

The production of reactive oxygen species (ROS) in biological systems has been associated with the pathogenesis of various diseases.[1−4] Since inorganic anions are ubiquitous in most biological and environmental systems, the interaction of these species with ROS, such as hydroxyl radical ($HO^{\bullet}$), may lead to the production of highly oxidizing radical species that can be detrimental to cell viability. The carbonic acid−bicarbonate ion equilibrium plays an important role in maintaining pH in blood plasma.[5−7] It has been shown that carbonate radical anion ($CO_3^{\bullet-}$) formation causes oxidative damage to copper or zinc superoxide dismutase (SOD1),[8] or it can stimulate SOD1 peroxidase activity in the presence of cysteine[9] or H_2O_2.[10] Moreover, $CO_3^{\bullet-}$ has been found to be produced from HCO_3^- during the turnover[11] of xanthine oxidase or as a bactericidal species during γ-irradiation.[12]

Electron paramagnetic resonance (EPR) spin trapping[13−19] has been an indispensable tool in the detection of oxygen radical species using the nitrone 5,5-dimethyl-1-pyrroline *N*-oxide (DMPO),[18−24] which has been widely employed as a spin trap in the detection of transient radicals in chemical or biological systems. The characteristic EPR spectrum arising from the formation of the spin adduct is used for the unambiguous identification of specific free radicals.

So far, the direct detection of $CO_3^{\bullet-}$ using DMPO as a spin trap has been achieved from simple systems by γ-irradiation of HCO_3^-/CO_3^{2-} buffer,[12] but there have been attempts to indirectly detect $CO_3^{\bullet-}$ using DMPO by detection of secondary products in vitro.[8−11,25−27] It is therefore important to determine the spin-trapping characteristics of $CO_3^{\bullet-}$ to accurately interpret the resulting EPR spectra during their formation in complex chemical and biological systems. This study will characterize the spin-trapping process by DMPO and $CO_3^{\bullet-}$ generated from UV photolysis of Na_2CO_3 (or $NaHCO_3$),[21,28,29] in the presence of H_2O_2. Various modes of radical addition and the stabilities of spin adducts formed will be theoretically and experimentally assessed.

Experimental Methods

General Computational Methods. Density functional theory[30,31] was applied in this study to determine the optimized geometry, vibrational frequencies, and single-point energy of all stationary points.[32−35] The effect of aqueous solvation also was investigated using the polarizable continuum model

* Corresponding Authors: (F.A.V.) E-mail: frederick.villamena@osumc.edu. Fax: (614)-292-8454. (C.M.H.) E-mail: hadad.1@osu.edu. Fax: (614)-292-1685. (J.L.Z.) E-mail: jay.zweier@osumc.edu. Fax: (614)-247-7799.

† College of Medicine.

§ Department of Chemistry.

‡ Institute for Structural Chemistry.

10.1021/jp065692d CCC: $37.00
Published on Web 12/14/2006

(PCM).[36−40] All calculations were performed using Gaussian 03[41] at the Ohio Supercomputer Center. Single-point energies were obtained at the B3LYP/6-31+G** level based on the optimized B3LYP/6-31G* geometries, and the B3LYP/6-31+G**//B3LYP/6-31G* wave functions were used for natural population analyses (NPA).[42] These calculations used six Cartesian d functions. Geometry optimization with diffuse functions at the B3LYP/6-311+G* level of theory was performed to account for the negative charge character of the species being investigated using five d (pure) functions for these calculations. Stationary points for DMPO and its respective $CO_3^{\bullet-}$ adducts have zero imaginary vibrational frequency as derived from a vibrational frequency analysis (B3LYP/6-31G*). A scaling factor of 0.9806 was used for the zero-point vibrational energy (ZPE) corrections for the B3LYP/6-31G* and the B3LYP/6-311+G* levels.[43] Spin contamination for all of the stationary points of the radical structures was negligible (i.e., $0.75 < \langle S^2 \rangle < 0.77$) except for the DMPO−$CO_3$ value of 1.76. The weighting of the 3 DMPO−OCO_2 isomers was determined via a Boltzmann average as shown in eq 1.

$$N_j = \frac{g_j e^{(-G_j/k_B T)}}{\sum_i g_i e^{(-G_j/k_B T)}} \quad (1)$$

In eq 1, G_i is the free energy at 298 K of structure i at the B3LYP/6-31+G**//B3LYP/6-31G* level, relative to the structure with the lowest free energy set as zero, g_i is the structural degeneracy, k_B is Boltzmann's constant, and T is temperature (298 K). For the free energy calculations, the vibrational frequencies were unscaled.

EPR Measurements. EPR measurements were carried out on an X-band spectrometer with high sensitivity (HS) resonator at room temperature. General instrument settings are as follows unless otherwise noted. EPR parameters: microwave power, 20 mW; modulation amplitude, 1 G; receiver gain, 2.00×10^4; sweep time, 42 s; and time constant, 10 ms. Simulation of spectra was performed using the program developed by Rockenbauer, et al.[44] The concentration of the spin adduct is based on 10 μM 2,2,5,5-tetramethyl-4-piperidin-1-oxyl (TEMPO) standard and was determined by computer simulation of the spectra that offered an amplitude data proportional to the concentration. The absolute concentrations are based on the same experimental conditions and the spectrometer settings (i.e., modulation field, amplification, microwave power, scan number) used for the standard.

Spin Trapping Studies. DMPO (99.9%), Na_2CO_3 (99.9%), $NaHCO_3$ (99.9%), 30% H_2O_2 in water, and an isotopic mixture of 80% $H_2{}^{17}O_2$−20% $H_2{}^{16}O_2$ in water were obtained commercially. All solutions were prepared using deoxygenated, double-distilled water. In a typical experiment, a final volume of 50 μL was used for EPR measurement and the solution was loaded into a 50 μL quartz micropipette. Carbonate radical anion was generated from irradiation[28] with a low-pressure mercury vapor lamp at a 254 nm wavelength of 100 mM aqueous solutions Na_2CO_3 or $NaHCO_3$ in the presence of the 25−50 mM DMPO and 10 μM (or 58 mM) H_2O_2. EPR spectra were acquired over the course of 45 min.

Griess Assay. A solution of 100 mM Na_2CO_3 in H_2O (pH ∼ 11) was titrated with 1 N hydrochloric acid to pH values of 10, 9, 8, and 7. A typical 100 μL solution consisting of 25 mM DMPO, 10 mM H_2O_2, and Na_2CO_3 at various pH values was irradiated by UV light for 15 min in quartz capillary tubes. Through the use of a Griess assay kit (Promega), a 50 μL aliquot of the irradiated solution was transferred in a 96-well cell culture cluster and was allowed to incubate with the appropriate reagents. The nitrite concentration was determined spectrophotometrically at 550 nm and with a molar absorptivity of (8.75 ± 1.2) × 10^3 L mol^{-1} cm^{-1}.[45] An average of 1.5 μM background NO_2^- concentration was observed from solutions containing only CO_3^{2-} at various pH levels, and this value was used to correct all of the NO_2^- readings. Concentrations were interpolated from a $NaNO_2$ standard curve. This was repeated for solutions without CO_3^{2-} by using water to titrate 1 N KOH to pH values of 11, 10, 9, 8, and 7. An average of 1.5 μM background NO_2^- concentration also was observed from solutions containing only KOH at various pH values and was used to correct all of the subsequent readings.

Gas Chromatograph−Mass Spectrometry (GC−MS) Analysis. Through the use of the same solutions used for Griess assay, a 50 μL aliquot of the aqueous mixture was extracted with 20 μL of $CHCl_3$. A 2 μL sample was injected into a 15 m

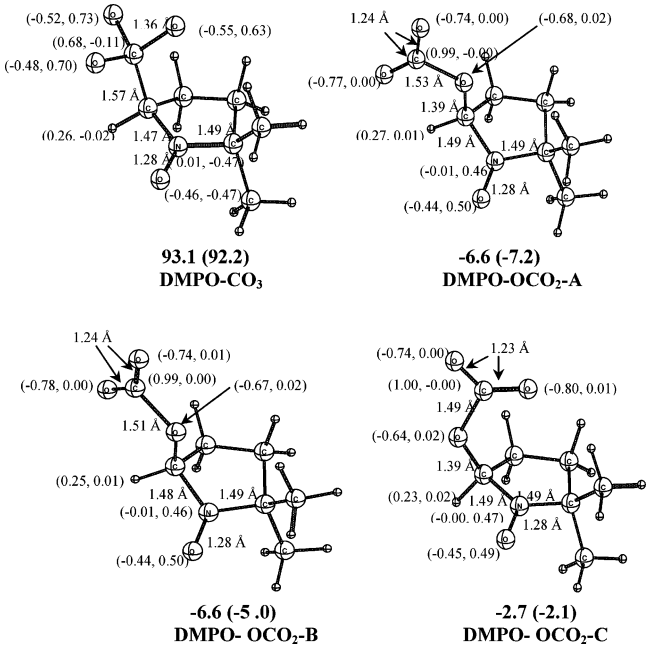

Figure 1. Bond distances and charge and spin density population (in parentheses) of various products arising from the addition of $CO_3^{\bullet-}$ addition to DMPO at the B3LYP/6-31+G**//B3LYP/6-31G* level. Also shown are aqueous-phase free energies of reaction ($\Delta G_{298K,aq}$ in kcal/mol) at the PCM/B3LYP/6-311+G* and PCM/B3LYP/6-31+G**//B3LYP/6-31G* (in parentheses) levels of theory.

TABLE 1: Aqueous Phase Reaction Enthalpies ($\Delta H_{298K,aq}$) and Free Energies ($\Delta G_{298K,aq}$) for Various Modes of $CO_3^{\bullet-}$ Addition to DMPO at the PCM/B3LYP/6-311+G* Level in kcal/mol

entry	$\Delta H_{298K,aq}$	$\Delta G_{298K,aq}$
	$CO_3^{\bullet-}$ + DMPO	
DMPO−CO_3	180.6	93.1
DMPO−OCO_2-A	−18.4	−6.6
DMPO−OCO_2-B	−18.4	−6.6
DMPO−OCO_2-C	−15.7	−2.7
	Scheme 2	
A[a]	18.2	8.0
B	6.7	7.5
C[a]	−14.9	−16.7
D[a]	−5.6	−6.5
E	37.3	37.3
F	−4.7	5.5

[a] Based on the most preferred structure DMPO−OCO_2−B.

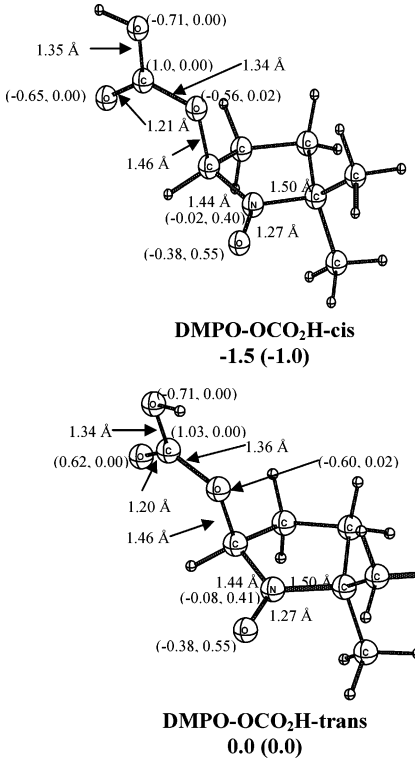

Figure 2. Bond distances and charge and spin density population (in parentheses) of protonated DMPO−OCO_2 at the B3LYP/6-31+G**// B3LYP/6-31G* level. Also shown are the relative gas and aqueous (in parentheses) phase free energies (ΔG_{298K} in kcal/mol) at the PCM/ B3LYP/6-31+G**//B3LYP/6-31G* level.

SCHEME 1: Acid−Base Equilibrium for the DMPO−OCO_2 and DMPO−OH Adducts

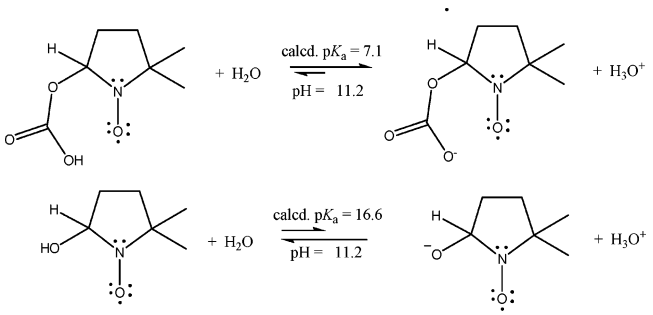

× 0.25 mm ID × 0.25 μm 5% phenyl−95% dimethylpolysiloxane column with an initial temperature of 40 °C. A linear gradient of temperature increase of 20 °C/min from 40 to 250 °C was used. Electron impact ionization (EI) analyses were conducted at 200 °C for the ion source temperature, an electron energy of 70 eV, and a scan speed of 1.6584 scans/s.

Results and Discussion

Electronic and Structural Analysis. Our predicted structure at the B3LYP/6-31+G** level for the carbonate radical anion ($CO_3^{\bullet-}$) gave a trigonal planar geometry with C_s symmetry. NPA atomic charges for $CO_3^{\bullet-}$ yielded a −0.64 e charge on each of the 3 O atoms and a +0.93 e positive charge on the C atom. The calculated C−O bond lengths in $CO_3^{\bullet-}$ gave a bond distance of 1.28 Å, consistent with the experimental C−O bond distance in $Na_2(CO_3)(H_2O)$[46] of 1.277 (4) Å. Unlike in $CO_2^{\bullet-}$ in which the spin population is mostly distributed on the C atom (~68%), there is no spin population on the C-atom in $CO_3^{\bullet-}$ (~ −0.06 e). Instead, the spin density is localized on the O atoms with each atom having a spin population of ~35%. We recently have completed a spin-trapping study of $CO_2^{\bullet-}$ with DMPO, and we noted in that work that a DMPO−CO_2 adduct was formed.[47] Because of the differences in spin population as well as charge density distribution between $CO_2^{\bullet-}$ and $CO_3^{\bullet-}$, it is interesting to investigate the mechanism of DMPO−CO_3 adduct formation compared to that of DMPO−CO_2 and to determine if the mode of radical addition to DMPO (i.e., whether O− or C-centered adduct) is governed by the charge density or spin population on the reacting radical.

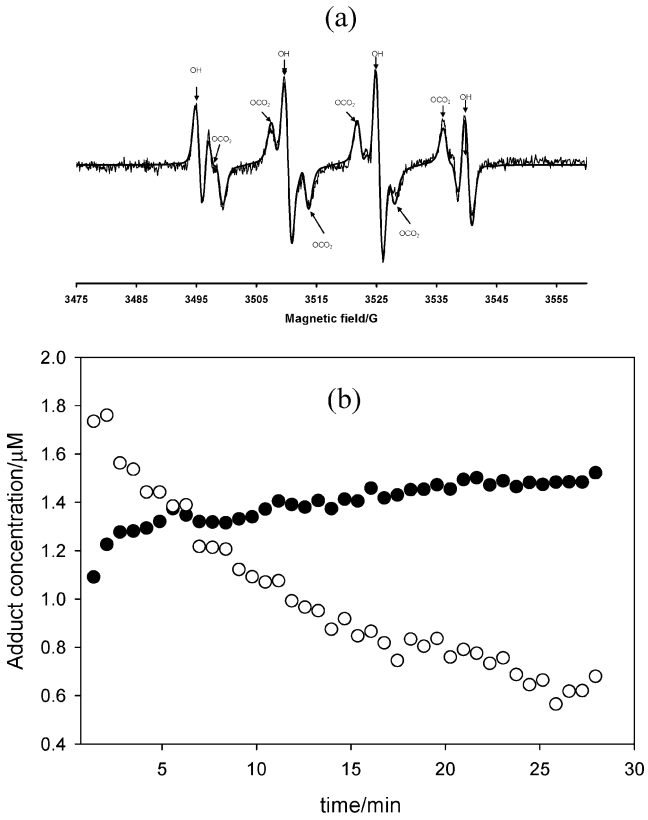

Figure 3. (a) X-band EPR spectrum of the carbonate radical anion ($CO_3^{\bullet-}$) addition to DMPO by UV photolysis of 58 mM $H_2{}^{16}O_2$ and 50 mM DMPO in the presence of 100 mM Na_2CO_3 showing the formation of a DMPO−OCO_2 and DMPO−OH adducts. Trace lines are simulations of the spectrum. (b) Plots of DMPO−OCO_2 decay (○) and DMPO−OH formation (●). See Experimental Methods for the EPR parameters used.

Figure 1 shows the various optimized adduct geometries resulting from the addition of $CO_3^{\bullet-}$ to DMPO. Two major types of products were predicted for the addition of $CO_3^{\bullet-}$ to DMPO, a C− and an O-centered radical adduct. From Table 1, it can be seen that the latter is more preferred by $\Delta G_{298K,aq} = -6.6$ kcal/mol as compared to the C-centered radical adduct with $\Delta G_{298K,aq} = 93.1$ kcal/mol. It should be noted that the spin contamination on DMPO−CO_3 is quite extensive with $\langle S^2 \rangle$ of 1.76 (Table S3, Supporting Information).[48] The spin (density) population on the carbonate-O atoms of DMPO−CO_3 range from 0.63 to 0.73 e with no spin population on either the nitroxyl-N and -O atoms. This suggests that the unpaired electron is localized mainly on the carbonate moiety, although the N−O and C−N bond distances are consistent with that found in nitroxides.[49] The endoergicity of formation of DMPO−CO_3 could be due to several factors: (1) absence of spin density on the carbonate-C atom of the $CO_3^{\bullet-}$ radical; (2) less favorable formation of a tetrahedral adduct than a bent adduct due to steric factors; (3) formation of the C−O bond is more favored as

TABLE 2: Calculated Isotropic Hyperfine Coupling Constants (hfcc values) in Gas and Aqueous Phases at the B3LYP/6-31+G Level of N, β-H, and γ-H of Various DMPO Spin Adducts Using the B3LYP/6-31G* Optimized Geometry**

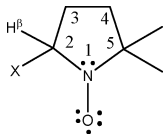

	isotropic hyperfine splitting constants (G)		
adduct	Nitronyl-N	β-H	γ-H[d]
	theoretical		
DMPO−OH[a]	11.69	5.92	0.88 (trans)
DMPO−OH·$(H_2O)_2$[b,c]	12.89	9.38	1.29 (cis)
			0.96 (trans)
DMPO−O_2H[a,b]	11.69	6.57	1.05 (trans)
DMPO−O_2H·$(H_2O)_2$[b,c]	11.76	13.62	0.84 (cis)
DMPO−CO_3[a]	11.07	10.3	1.66 (trans)
DMPO−OCO_2-A[a]	12.11	4.26	1.43 (trans)
			1.46 (cis)
DMPO−OCO_2-B[a]	11.89	3.95	1.14 (trans)
			1.37 (cis)
DMPO−OCO_2-C[a]	11.64	11.68	1.26 (cis)
DMPO−OCO_2[a,b]	11.95	4.23	1.21 (trans)
			1.40 (cis)
DMPO−OCO_2H[a]	8.48	5.86	1.17 (trans)
			1.73 (cis)
	experimental		
$CO_3^{\bullet-}$ + DMPO[e]	15.00	14.81	
	14.32	10.68	1.37
DMPO−OH[f]	15.00	14.75	
DMPO-^{17}OH[g]	14.98	14.72	^{17}O = 4.65
			^{13}C(2) = 5.3
			^{13}C(2) = 7.0 G
DMPO−O_2H[f]	14.3	11.7	1.25

[a] Predicted gas-phase hfcc values at the B3LYP/6-31+G** level. [b]Boltzmann weighted. [c]Predicted aqueous phase hfcc with 2 explicit water molecules at the PCM/B3LYP/6-31+G** level. The Δa_x (defined as $a_{aq} - a_{gas}$) for the effect of solvation on hfcc for DMPO−OH are $\Delta a_N = 1.20$ G and $\Delta a_{\beta-H} = 3.46$ G, although for DMPO−O_2H the values are $\Delta a_N = -0.11$ G and $\Delta a_{\beta-H} = 7.02$ G.[53] [d]Predicted isotropic hyperfine coupling constants for γ-H values at the C-3 position; cis/trans indicate position of γ-H relative to the $-CO_3$, $-$OH or $-O_2$H moieties. [e]Two species were observed with g = 2.00679 and 2.00671 corresponding to DMPO−OCO_2 and DMPO−OH adducts, respectively. [f]The Δa_x correction (defined as $a_{exptl} - a_{calcd,gas}$) for DMPO−OH are $\Delta a_N = 3.31$ G and $\Delta a_{\beta-H} = 8.83$ G, although for DMPO−O_2H the values are $\Delta a_N = 2.43$ G and $\Delta a_{\beta-H} = 5.1$ G. The Δa_x correction (defined as $a_{exptl} - a_{calcd,aq}$) for DMPO−OH are $\Delta a_N = 2.11$ G and $\Delta a_{\beta-H} = 5.38$ G, although for DMPO−O_2H the values are $\Delta a_N = 2.54$ G and $\Delta a_{\beta-H} = -1.97$ G. [g]With DMPO−H adduct contamination (2−3%).

compared to the C−C bond because of differences in the C−O and C−C bond dissociation energies.[50]

Three optimized conformational isomers were predicted for the O-centered adducts: DMPO−OCO_2-A, DMPO−OCO_2-B, and DMPO−OCO_2-C (Figure 1). Two of the conformational isomers, DMPO−OCO_2-A and DMPO−OCO_2-B, have the $-CO_2$ group oriented away from the ring system, while DMPO−OCO_2-C has the $-CO_2$ group oriented toward the ring system. The formation of DMPO−OCO_2-A and DMPO−OCO_2-B adducts are the most exoergic with $\Delta G_{298K,aq} = -6.6$ kcal/mol, while the formation of DMPO−OCO_2-C is the least exoergic with $\Delta G_{298K,aq} = -2.7$ kcal/mol perhaps due to a steric effect between the $-CH_3$ and $-CO_2$ groups in DMPO−OCO_2-C. A $C_{ring}-O-C_{CO2}$ bond angle of 114.7° was predicted for DMPO−OCO_2-B, while 116.3° and 120° was predicted for DMPO−OCO_2-A and DMPO−OCO_2-C, respectively. No significant spin population was obtained on the carbonate-O's for all of the O-centered adducts, while spin populations of 0.46 and 0.50 e for the nitroxyl-N and -O, respectively, were predicted and generally are consistent with spin populations in nitroxides. The C−N and N−O bond distances for the O-centered adducts also were consistent with reported experimental bond distances for nitroxides.[49] These results suggest that the atomic charge on the radical reactant does not play a significant role on the mode of radical addition to DMPO.

To establish the major form of the DMPO−OCO_2 adduct in solution, the cis and trans structures of DMPO−OCO_2H were optimized (Figure 2). Unlike the DMPO−CO_2H adduct,[47] the cis isomer of DMPO−OCO_2H is preferred in both gas and

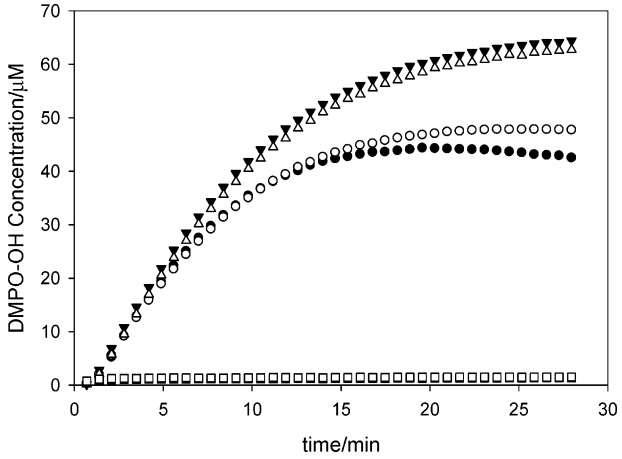

Figure 4. Formation of DMPO−OH adduct by UV photolysis of 50 mM DMPO and 58 mM H_2O_2 alone (△,▼) and in the presence of 100 mM $NaHCO_3$ (●, ○) or 100 mM Na_2CO_3 (■, □) in distilled water. See Experimental Methods for the EPR parameters used.

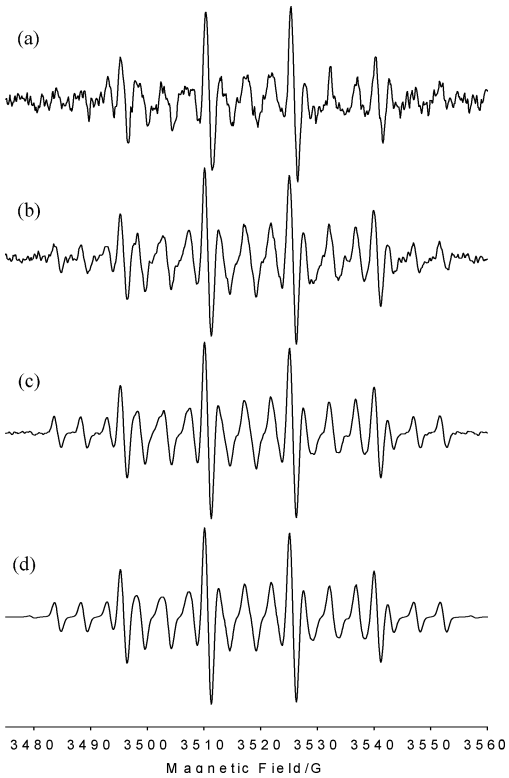

Figure 5. X-band EPR spectrum resulting from the UV photolysis of (a) 10 μM (80/20%) $H_2{}^{17}O_2$/ $H_2{}^{16}O_2$ and 50 mM DMPO in the presence of 100 mM Na_2CO_3; (b) in the presence of 100 mM $NaHCO_3$; (c) same as in (a) and (b) but in the absence of anions; (d) simulated spectrum of (c). See Experimental Methods for the EPR parameters used.

SCHEME 2: Mechanisms for the DMPO−OH Formation from DMPO−OCO_2

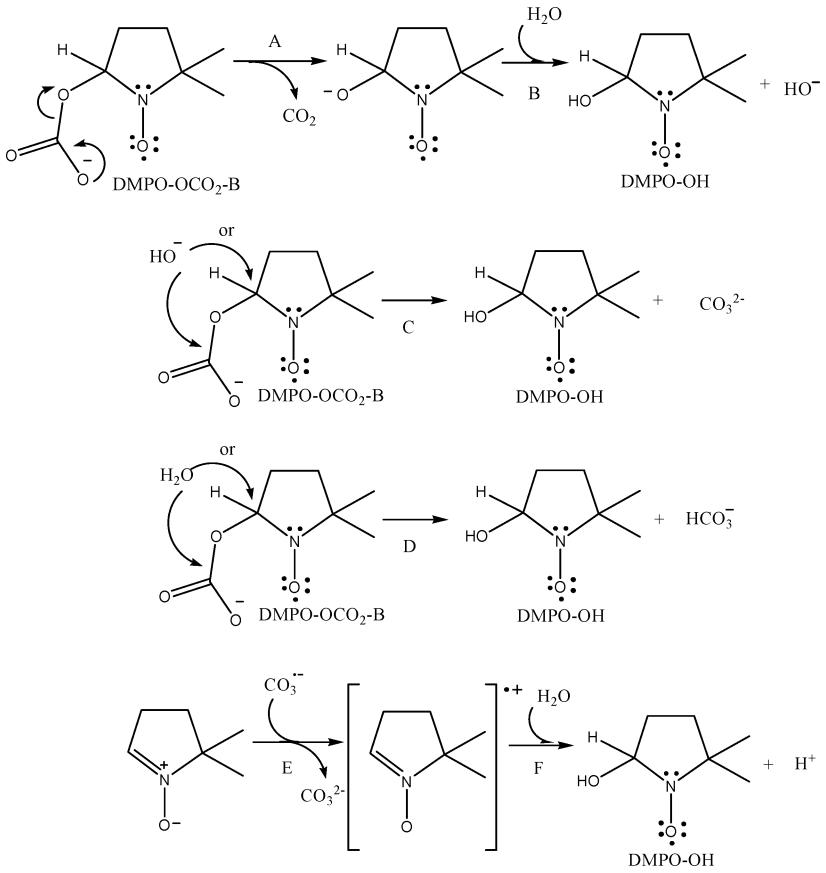

aqueous phases by about 1.0 kcal/mol. It is worth noting that the $C_{CO2H}-O_{ring}$ bond distances in DMPO−OCO_2H (which range from 1.34 to 1.36 Å) is significantly shorter compared to the $C_{CO2}-O_{ring}$ bond distances (1.49−1.53 Å) in the unprotonated adduct, DMPO−OCO_2. However, the $O_{CO3H}-C_{ring}$ bond distance is longer in DMPO−OCO_2H compared to that in the unprotonated form (i.e., 1.46 Å versus 1.39 Å). The long $C_{CO2}-O_{ring}$ bond distances in the unprotonated DMPO−OCO_2 adducts may have an important role in the decomposition of the adduct in basic media as will be discussed in the next section.

On the basis of the optimized DMPO−OCO_2H structures, the pK_a of DMPO−OCO_2H was calculated, and the pK_a was approximated to be 7.1 and is close to the reported[51,52] pK_a of $HOCO_2H$ of 6.4 (see Table S2 and Figure S1, Supporting Information). Therefore, at pH 11, it is expected that the anionic form of DMPO−OCO_2H will be the major form in solution (Scheme 1).

EPR Spin Trapping. Figure 3a shows the spectrum arising from the UV photolysis of 58 mM H_2O_2 in the presence of 100 mM Na_2CO_3 and 50 mM DMPO. The major spectrum is characteristic of a DMPO−OH adduct with $g = 2.00671$, $a_N =$ 15.00 G, and $a_{\beta-H} = 14.81$ G, while a minor species with $g =$ 2.00679 also was observed with $a_N = 14.32$ G, $a_{\beta-H} = 10.68$ G, and $a_{\gamma-H} = 1.37$ G but is relatively short lived as shown by the decay plot in Figure 3b. The *g*-factor and the a_N for the observed minor peak at $g = 2.00679$ are characteristic of an O-centered radical adduct. However, with the $a_{\beta-H} = 10.68$ G being 1 G smaller than what is expected for DMPO−O_2H (i.e., $a_{\beta-H} = 11.70$ G), the signal can be assigned to a new species, perhaps that of DMPO−OCO_2. We attempted to interpret the experimental hyperfine coupling constant (hfcc) values initially assigned to DMPO−OCO_2 with a theoretical approach by calculating the hfcc values at the B3LYP level of theory. The Boltzmann-weighted gas-phase hfcc values of the three O-centered adducts shown in Figure 1 gave $a_N = 11.95$ G, $a_{\beta-H} =$ 4.23 G, and $a_{\gamma-H} = 1.21-1.40$ G, which are close to the predicted gas-phase hfcc values of DMPO−OH of $a_N = 11.69$ G, $a_{\beta-H} = 5.92$ G, and $a_{\gamma-H} = 0.88$ G (based on only one preferred conformer), or the Boltzmann weighted average hfcc values for DMPO−O_2H of $a_N = 11.69$ G, $a_{\beta-H} = 6.57$ G, and $a_{\gamma-H} = 1.08$ G (see Table 2). Although the predicted hfcc values for DMPO−OCO_2 are within the error limits (i.e., theoretical versus experimental hfcc) predicted for DMPO−OH or DMPO−O_2H from our previously reported study,[53] a qualitative trend between theoretical and experimental hfcc values can be seen. For example, the predicted Boltzmann weighted $a_{\beta-H}$ for DMPO−OCO_2 of 4.23 G is lower than that predicted for DMPO−O_2H of 6.57 G and follows the same qualitative trend with the experimental hfcc values of 10.68 and 11.7 G for the species of interest and DMPO−O_2H, respectively. The same qualitative trend can also be seen for the predicted and experimental $a_{\gamma-H}$ in which DMPO−OCO_2 exhibits larger $a_{\gamma-H}$ than that of DMPO−O_2H. On the basis of these predicted gas-phase and experimental hfcc values for DMPO−OH and DMPO−O_2H, it is reasonable to assume that the observed minor peak at $g = 2.00679$ arising from UV photolysis of H_2O_2 in the presence of Na_2CO_3 and DMPO is probably due to the formation of the DMPO−OCO_2 adduct.

Figure 4 shows the evolution of the DMPO−OH EPR spectrum in the absence and presence of Na_2CO_3 or $NaHCO_3$ and also shows that the formation of DMPO−OH is significantly diminished in the presence of Na_2CO_3 or $NaHCO_3$ even at high H_2O_2 concentration (58 mM). The formation of the DMPO−OH adduct as a minor product in an attempt to trap $CO_3^{\bullet-}$ with DMPO raises interesting questions as to whether DMPO−OH is formed in a competitive manner between

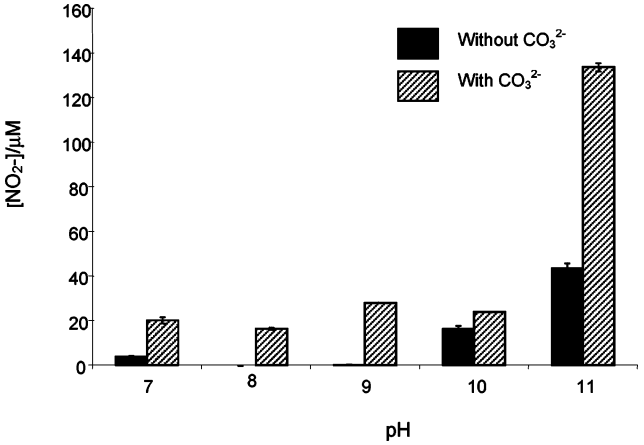

Figure 6. Griess assay of nitrite formation as a function of pH from the UV photolysis of 25 mM DMPO, 10 mM H_2O_2, and 100 mM Na_2CO_3 (titrated with HCl). In a control experiment, nitrite formation was not observed in the absence of UV light under the same experimental conditions.

DMPO and CO_3^{2-} along with the initially formed $HO^\bullet$ or if the observed DMPO−OH signal is due to a secondary product formed from the decomposition of the initially formed DMPO−OCO_2 adduct. The significant loss in EPR signal in the presence of Na_2CO_3 or $NaHCO_3$ also raises interesting questions as to the possible mechanism of $CO_3^{\bullet-}$ addition to DMPO, the stability of the DMPO−OCO_2 adduct, and its final fate in aqueous solution. Answers to these questions are critical for the accurate interpretation of EPR spectra arising from the spin trapping of $CO_3^{\bullet-}$ by DMPO.

To confirm if the observed "DMPO−OH-like" EPR spectrum originates from the direct trapping of $HO^\bullet$ by DMPO to form the DMPO−OH adduct and not from DMPO−OCO_2, an 80% enriched sample of O-17 labeled $H_2{}^{17}O_2$ was used and showed the formation of DMPO-^{17}OH with $a_N = 14.98$ G, $a_{\beta-H} = 14.72$ G, and $a_{O-17} = 4.65$ G using either Na_2CO_3 or $NaHCO_3$ (Figure 5a,b, respectively). These experiments, therefore, confirm the identity of the major-formed adduct as DMPO−OH as derived from the direct spin trapping of the initially generated $H^{17}O^\bullet$ with DMPO. This is supported by a previous study[54] that showed that trapped $H^{17}O^\bullet$ is derived exclusively from $H_2{}^{17}O_2$ with no isotopic scrambling between $H_2{}^{17}O_2$ and water solvent. Because of significant signal overlap between the DMPO−OCO_2 adduct and that of the DMPO-^{17}OH adduct and exacerbated by the low intensity of the formed DMPO−OCO_2 adduct, it was not possible to observe the formation of the DMPO−OCO_2 adduct using $H_2{}^{17}O_2$. Competitive kinetic studies also confirmed the direct $HO^\bullet$ addition to DMPO in the presence of Na_2CO_3 or $NaHCO_3$ and is further discussed in the Supporting Information.

Theoretical Routes for DMPO−OH Formation from DMPO−OCO_2. There have been experimental studies on the enzyme-mediated[8−11] generation of $CO_3^{\bullet-}$, but there was no direct evidence for the spin trapping of $CO_3^{\bullet-}$ by DMPO as detected by EPR, although several mechanisms have been proposed for the formation of the DMPO−OH adduct from the enzymatic generation of $CO_3^{\bullet-}$ in the absence of free $HO^\bullet$. The nucleophilic substitution of the carbonate moiety in DMPO−OCO_2 by H_2O was proposed by Zhang et al.,[10] while nucleophilic addition of H_2O to a radical cation DMPO intermediate was proposed by Bonini et al.[11] To give insight into other possible pathways for the formation of DMPO−OH other than direct addition of $HO^\bullet$ to DMPO and to explain the short half-life of DMPO−OCO_2 in aqueous solution,

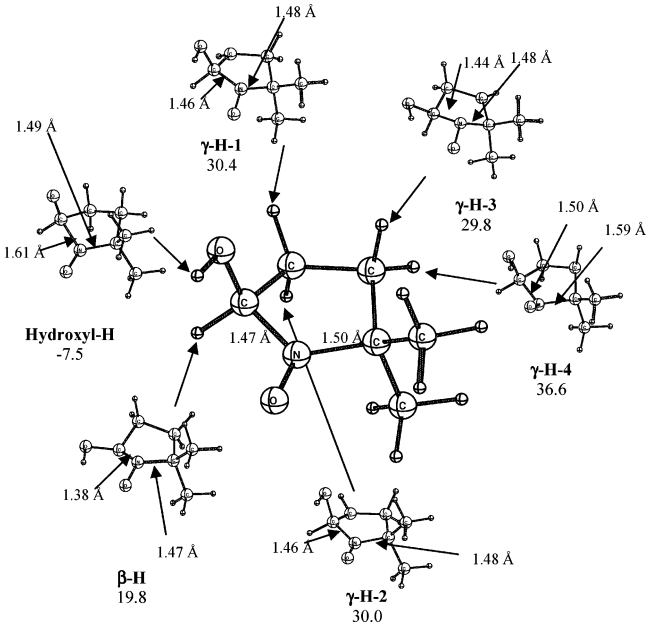

Figure 7. Aqueous phase free energies of reaction ($\Delta G_{298K,aq}$ in kcal/mol) of various products arising from the proton abstraction from various sites of the DMPO−OH adduct at the PCM/B3LYP/6-311+G* level. Note the increase in the C−N bond length upon deprotonation of the hydroxyl-H, which can lead to ring opening.

the thermodynamics of DMPO−OH formation from the DMPO−OCO_2 adduct is presented.

Three possible mechanisms were considered for the formation of DMPO−OH as shown in Scheme 2: (1) $C_{CO2}-O_{ring}$ bond cleavage to yield an alkoxide with subsequent proton abstraction from water (reaction A and B); (2) nucleophilic substitution of the carbonate group by HO^- (reaction C) or by water (reaction D); (3) oxidation of DMPO by $CO_3^{\bullet-}$ to form a DMPO radical cation intermediate (reaction E) followed by nucleophilic addition of H_2O (reaction F). Table 1 shows that the most thermodynamically favorable pathway for the formation of the DMPO−OH adduct is via nucleophilic substitution of the carbonate moiety by HO^- or H_2O according to reactions C and D (Scheme 2), with $\Delta G_{298K,aq}$ of −16.7 and − 6.5 kcal/mol, respectively. Compared to other pathways, which are highly endoergic, (i.e., for reaction A, $\Delta G_{298K,aq} = 8.0$ kcal/mol and for reaction E, $\Delta G_{298K,aq} = 37.3$ kcal/mol (Table 1)), reactions C and D are most likely to occur in solution. However, although the overall $\Delta G_{298K,aq}$ for the formation of DMPO−OH via the DMPO−OCO_2 adduct is −23.3 kcal/mol (i.e., −6.6 kcal/mol (DMPO + $CO_3^{\bullet-}$) and −16.7 kcal/mol (reaction C)), the formation of DMPO−OH adduct from direct $HO^\bullet$ addition to DMPO is more exoergic with $\Delta G_{rxn,aq} = -38.3$ kcal/mol. On the basis of these calculated thermodynamic values, it appears that for DMPO−OH to be formed from DMPO−OCO_2, the concentration of exogenous $HO^\bullet$ should be negligible and that the $CO_3^{\bullet-}$ production occurs other than by direct oxidation of CO_3^{2-}/HCO_3^- by $HO^\bullet$.

Furthermore, Sauers and co-workers[55] have studied the equilibrium reaction of a series of aliphatic alcohols of varying pK_a with HCO_3^- (eq 2). The experimental K_{eq} was found to be approximately 0.13 indicating that the position of the equilibrium points to the breakdown of alkyl monocarbonates to the corresponding alcohol.

$$ROH + HCO_3^- \overset{K_{eq}\sim 0.13}{\rightleftharpoons} ROCO_2^- + H_2O \qquad (2)$$

It can therefore be inferred that in the absence of exogenous $HO^{\bullet}$, the formation of the DMPO−OH adduct from the addition of $CO_3^{\bullet-}$ to DMPO is a result of nucleophilic substitution of HO^- or H_2O to the DMPO−OCO_2 adduct.

Product Analysis. Product analysis of the reaction mixture after generation of $CO_3^{\bullet-}$ in the presence of DMPO was carried out using GC-MS and Griess assay, and results revealed a distinctive GC peak with a nominal mass of 98 *m*/*z* and formation of nitrite anion (NO_2^-), respectively. A discussion on the characterization of the 98 *m*/*z* peak is presented in detail in the Supporting Information, although its actual structure has not been successfully identified. Furthermore, NO_2^- formation has been shown to be dependent on both pH as well as the presence of CO_3^{2-} (Figure 6). The formation of NO_2^- in the absence of CO_3^{2-} can originate from the oxidation of reactive nitrogen species (RNS) that are released upon proton abstraction of the hydroxyl-H from the DMPO−OH adduct, perhaps via a ring-opening mechanism as demonstrated in our previous work.[56] The proton abstraction of the hydroxyl-H ($\Delta G_{298K,aq} = -7.5$ kcal/mol) is most favored compared to the abstraction of the methylene-H ($\Delta G_{298K,aq} = 29.8$ to 36.6 kcal/mol) or the methine-H ($\Delta G_{298K,aq} = 19.8$ kcal/mol) (Figure 7). Further discussion on the acidity of the DMPO−OH adduct is discussed in the Supporting Information.

Conclusions

Theoretical studies show that the preferred mode of $CO_3^{\bullet-}$ addition to DMPO is the formation of an O-centered radical (DMPO−OCO_2) adduct as governed mostly by the spin population on the reacting $CO_3^{\bullet-}$ radical; furthermore, the atomic charge distribution only plays a minor role in determining the type of adduct formed. The formation of a C-centered adduct from $CO_3^{\bullet-}$ is unfavorable due to steric factors as well as the low spin density distribution on the carbonate-C. EPR spin-trapping experiments show formation of DMPO−OCO_2 along with DMPO−OH during irradiation of H_2O_2 and DMPO in the presence of CO_3^{2-} or HCO_3^-. The formation of DMPO−OH was found to be a result of direct addition of $HO^{\bullet}$ to DMPO as supported by isotope-labeling experiments. The formation of the DMPO−OH adduct from DMPO−OCO_2 in the absence of free $HO^{\bullet}$, as in the case of enzyme-mediated generation of $CO_3^{\bullet-}$, or as possible secondary product of DMPO−OCO_2 was theoretically investigated. Results show that the nucleophilic substitution of the carbonate moiety of DMPO−OCO_2 by H_2O (or HO^-) is the most favorable pathway. Product analysis of the spin trapping reaction of DMPO with $CO_3^{\bullet-}$ shows formation of NO_2^- and is dependent mainly on CO_3^{2-} concentration with minor effect from the basicity of solution.

The favorability of CO_3^{2-} ($\Delta G_{298K,aq} = -6.6$ kcal/mol) addition to DMPO is close to that reported for hydroperoxyl ($HO_2^{\bullet}$) ($\Delta G_{298K,aq} = -7.9$ kcal/mol) radical addition to DMPO[57] suggesting that $CO_3^{\bullet-}$ reactivity can have biological significance and consequences for oxidative damage.

Acknowledgment. The authors thank The Ohio Supercomputer Center (OSC) for computational support of this research. This work was financially supported by NIH grants HL38324, HL63744, and HL65608. C.M.H. acknowledges financial support from the NSF-funded Environmental Molecular Science Institute (CHE-0089147) at The Ohio State University. A.R. acknowledges the Hungarian Scientific Research Fund Grant OTKA T-046953.

Supporting Information Available: Energies, enthalpies, and free energies for all spin traps and their corresponding spin adducts are available as Supporting Information, as is the complete citation for ref 44. This information is available free of charge via the Internet at http://pubs.acs.org.

References and Notes

(1) Halliwell, B. *Oxid. Stress Dis.* **2001**, *7*, 1.
(2) Halliwell, B. *Drugs Aging* **2001**, *18*, 685.
(3) Zweier, J. L.; Talukder, M. A. H. *Cardiovasc. Res.* **2006**, *70*, 181.
(4) Zweier, J. L.; Villamena, F. A. Chemistry of free radicals in biological systems. In *Oxidative Stress and Cardiac Failure*; Kukin, M. L., Fuster, V., Eds.; Futura Publishing: Armonk, NY, 2003; pp 67.
(5) Javaheri, S.; Nardell, E. A.; Kazemi, H. *Respir. Physiol.* **1979**, *36*, 155.
(6) Krapf, R.; Beeler, I.; Hertner, D.; Hulter, H. N. *N. Engl. J. Med.* **1991**, *324*, 1394.
(7) Wesson, D. E. *Am. J. Physiol.* **1996**, F132.
(8) Ramirez, D. C.; Gomez, M.; Sandra, E.; Mason, R. P. *Free Radical Biol. Med.* **2005**, *38*, 201.
(9) Karunakaran, C.; Zhang, H.; Joseph, J.; Antholine, W. E.; Kalyanaraman, B. *Chem. Res. Toxicol.* **2005**, *18*, 494.
(10) Zhang, H.; Joseph, J.; Felix, C.; Kalyanaraman, B. *J. Biol. Chem.* **2000**, *275*, 14038.
(11) Bonini, M. G.; Miyamoto, S.; Di, Mascio, P.; Augusto, O. *J. Biol. Chem.* **2004**, *279*, 51836.
(12) Wolcott, R. G.; Franks, B. S.; Hannum, D. M.; Hurst, J. K. *J. Biol. Chem.* **1994**, *269*, 9721.
(13) Karoui, H.; Hogg, N.; Frejaville, C.; Tordo, P.; Kalyanaraman, B. *J. Biol. Chem.* **1996**, *271*, 6000.
(14) Olive, G.; Mercier, A.; Le, Moigne, F.; Rockenbauer, A.; Tordo, P. *Free Radical Biol. Med.* **2000**, *28*, 403.
(15) Rosen, G. M.; Britigan, B. E.; Halpern, H. J.; Pou, S. *Free Radicals: Biology and Detection by Spin Trapping*; Oxford University Press: New York, 1999.
(16) Stolze, K.; Udilova, N.; Nohl, H. *Biol. Chem.* **2002**, *383*, 813.
(17) Villamena, F. A.; Zweier, J. L. *J. Chem. Soc., Perkin. Trans.* **2002**, *2*, 1340.
(18) Zweier, J. L.; Kuppusamy, P.; Lutty, G. A. *Proc. Natl. Acad. U.S.A.* **1988**, *85*, 4046.
(19) Zweier, J. L.; Kuppusamy, P.; Williams, R.; Rayburn, B. K.; Smith, D.; Weisfeldt, M. L.; Flaherty, J. T. *J. Biol. Chem.* **1989**, *264*, 18890.
(20) Gianni, L.; Zweier, J.; Levy, A.; Myers, C. E. *J. Biol. Chem.* **1985**, *260*, 68206.
(21) Czapski, G.; Lymar, S. V.; Schwarz, H. A. *J. Phys. Chem. A* **1999**, *103*, 3447.
(22) Villamena, F. A.; Hadad, C. M.; Zweier, J. L. *J. Am. Chem. Soc.* **2004**, *126*, 1816.
(23) Zweier, J. L.; Flaherty, J. T.; Weisfeldt, M. L. *Proc. Natl. Acad. U.S.A.* **1987**, *84*, 1404.
(24) Wang, P.; Chen, H.; Qin, H.; Sankarapandi, S.; Becher, M. W.; Wong, P. C.; Zweier, J. L. *Proc. Natl. Acad. Sci. U.S.A.* **1998**, *95*, 4556.
(25) Kochany, J.; Lipczynska-Kochany, E. *Chemosphere.* **1992**, *25*, 1769.
(26) Ramirez, D. C.; Mejiba, S. E. G.; Mason, R. P. *J. Biol. Chem.* **2005**, *280*, 27402.
(27) Yoon, J. H.; Jung, J.; Chung, H. H.; Lee, M. J. *J. Radioanal. Nucl. Chem.* **2002**, *253*, 217.
(28) Neta, P.; Huie, R. E.; Ross, A. B. *J. Phys. Chem. Ref. Data* **1988**, *17*, 1027.
(29) Wu, G.; Katsumura, Y.; Muroya, Y.; Lin, M.; Morioka, T. *J. Phys. Chem. A* **2002**, *106*, 2430.
(30) Labanowski, J. W.; Andzelm, J. *Density Functional Methods in Chemistry*; Springer: New York, 1991.
(31) Parr, R. G.; Yang, W. *Density Functional Theory in Atoms and Molecules*; Oxford University Press: New York, 1989.
(32) Becke, A. D. *Phys. Rev.* **1988**, *38*, 3098.
(33) Lee, C.; Yang, W.; Parr, R. G. *Phys. Rev. B* **1988**, *37*, 785.
(34) Becke, A. D. *J. Chem. Phys.* **1993**, *98*, 1372.
(35) Hehre, W. J.; Radom, L.; Schleyer, P. V.; Pople, J. A. *Ab Initio Molecular Orbital Theory*; John Wiley & Sons: New York, 1986.
(36) Barone, V.; Cossi, M.; Tomasi, J. *J. Chem. Phys.* **1997**, *107*, 3210.
(37) Barone, V.; Cossi, M.; Tomasi, J. *J. Comput. Chem.* **1998**, *19*, 404.
(38) Cossi, M.; Barone, V.; Cammi, R.; Tomasi, J. *Chem. Phys. Lett.* **1996**, *255*, 327.
(39) Tomasi, J.; Mennucci, B.; Cammi, R. *Chem. Rev.* **2005**, *105*, 2999.
(40) Tomasi, J.; Persico, M. *Chem. Rev.* **1994**, *94*, 2027.
(41) Frisch, M. J. *et al. Gaussian 03*, Revision B.04 ed.; Gaussian, Inc.: Pittsburgh, PA, 2003.
(42) Reed, A. E.; Curtiss, L. A.; Weinhold, F. A. *Chem. Rev.* **1988**, *88*, 899.
(43) Scott, A. P.; Radom, L. *J. Phys. Chem.* **1996**, *100*, 16502.
(44) Rockenbauer, A.; Korecz, L. *Appl. Magn. Reson.* **1996**, *10*, 29.

(45) Tsikas, D.; Gutzki, F.-M.; Rossa, S.; Bauer, H.; Neumann, C.; Dockendorff, K.; Sandmann, J.; Frolich, J. C. *Anal. Biochem.* **1997**, *244*, 208.

(46) Skakle, J. M. S.; Wilson, M. I.; Feldmann, J. *Acta. Crystallogr., Sect. E Struct. Rep. Online* **2001**, *E57*, i94.

(47) Villamena, F. A.; Locigno, E. J.; Rockenbauer, A.; Hadad, C. M.; Zweier, J. L. *J. Phys. Chem. A* **2006**, *110*, 13253−13258.

(48) Attempts to eliminate the spin contamination on DMPO-CO_3 using a diffuse function at the B3LYP/6−311+G* level did not improve the $<S^2>$ value.

(49) Boeyens, J. C. A.; Kruger, G. J. *Acta. Cryst.* **1970**, *B26*, 668.

(50) Lide, D. R. *CRC Handbook of Chemistry and Physics*; CRC Press: Boca Raton, FL, 1996.

(51) Schwarzenbach, G. *Helv. Chim. Acta.* **1957**, *40*, 907.

(52) Tossell, J. A. *Geochim. Cosmochim. Acta.* **2005**, *69*, 5647.

(53) Villamena, F. A.; Merle, J. K.; Hadad, C. M.; Zweier, J. L. *J. Phys. Chem. A.* **2005**, *109*, 6089.

(54) Lloyd, R. V.; Hanna, P. M.; Mason, R. P. *Free Radical Biol. Med.* **1997**, *22*, 885.

(55) Sauers, C. K.; Jencks, W. P.; Groh, S. *J. Am. Chem. Soc.* **1975**, *97*, 5546.

(56) Locigno, E. J.; Zweier, J. L.; Villamena, F. A. *Org. Biomol. Chem.* **2005**, *3*, 3220.

(57) Villamena, F. A.; Hadad, C. M.; Zweier, J. L. *J. Phys. Chem. A* **2005**, *109*, 1662.